J. Fluid Mech. (2003), *vol.* 495, *pp.* 369–384.
DOI: 10.1017/S0022112003006384 Printed in the United Kingdom

A mixing-length model for shallow turbulent wakes

By PETER K. STANSBY

Manchester Centre for Civil and Construction Engineering, UMIST, Manchester M60 1QD, UK

(Received 8 November 2002 and in revised form 28 July 2003)

A three-dimensional boundary-layer model of shallow-water flows assuming hydrostatic pressure with negligible numerical diffusion and wave damping has been extended to turbulent flow. A standard two-layer mixing-length model determines vertical length scales. The horizontal mixing length is made a multiple β of the vertical value and β is determined from comparison with experiment. Eddy viscosity is of a general three-dimensional form where, for example, the horizontal mixing length and associated strain rates determine the magnitude of eddy viscosity and hence vertical mixing (and vice versa). Direct comparison is made with previous experiments for subcritical flow around a conical island of small side slope which exhibits the transition from a vigorous vortex-shedding wake to a steady recirculating wake as the stability parameter, St, is increased. The value of β influences wake structure, particularly for stability parameters close to the critical (the value at which the wake becomes steady or stable). The critical value in the experiments was 0.4 and this was reproduced in the model with $\beta = 6$. Vortex shedding patterns with $St = 0.26$ and 0.36 were qualitatively reproduced. The flows were subcritical with an onset Froude number of about 0.2, with values approaching 0.6–0.7 in areas where depth-averaged vorticity magnitude was also greatest, at a small distance from the wet/dry intersection. At this intersection, depth-averaged vorticity approached zero while potential vorticity (depth-averaged vorticity/depth) was at a maximum, indicating the importance of the intersection as an origin for vorticity.

1. Introduction

Shallow-water flows, where the horizontal length scales are much larger than the vertical depth-limited scales, occur in coastal regions, estuaries and rivers. The subject has been reviewed in Jirka (2001). Modelling such flows by solving the shallow-water equations is common practice with several well-known commercial packages available. (Here 'modelling' implies numerical modelling.) Some components of these flows have been satisfactorily resolved, but here we consider problems associated with recirculations or wakes due to headlands, islands, sandbanks, etc. It is well known that model predictions for (unbounded) flows around bluff cylinders are sensitive to the advection scheme, the order of temporal and spatial discretization, mesh refinement (or lack of it) and the turbulence modelling strategy. In studies on shallow flows, there is increasing awareness of corresponding sensitivity as numerical schemes improve. In the past, first-order time stepping and relatively coarse grids have often made numerical diffusion and wave damping significant, swamping effects associated with turbulence modelling. In this paper, we are concerned with bed topographies of small slope and thus effects due to separation from 'steep', in the extreme vertical, surfaces

are not considered. Turbulence is bed-generated and horizontal recirculations are of a much larger scale. Without recirculation, attached turbulent flows may be adequately simulated by the mixing-length turbulence modelling of Prandtl (1927). The two-layer model is described in Rodi (1984) for steady flow and has been applied to unsteady flow by, for example, Cobbin, Stansby & Duck (1995). With recirculation, an appropriate turbulence modelling strategy for horizontal diffusion has yet to be established. Properly resolved three-dimensional large-eddy simulation (LES) or full Reynolds-stress-transport modelling are not yet practical propositions for such large-scale flows.

Depth-averaged modelling has been widely used in the past, and is still popular, enabling small horizontal scales to be resolved with limited computer resources. Rastogi & Rodi (1978) notably developed a $k-\varepsilon$ model with production of k and ε obtained by adding components due to bed generation and horizontal strain rates, effectively implying different horizontal and vertical length scales (k is turbulent kinetic energy and ε its dissipation rate.) k and ε then determine eddy viscosity. This has proved a useful pragmatic approach and has been widely applied with various empirical modifications. There is the limitation of all depth-averaged models concerning dispersion effects due to the non-uniform vertical variation of velocity. It has to be assumed that these effects are small or that a standard velocity profile, e.g. the 'log' profile, applies. Depth-averaged modelling will, of course, remain attractive if predictions are adequate or at least if its limitations can be defined.

This paper applies the three-dimensional shallow-water equations in (partially) conservative form with the assumption of hydrostatic pressure, which is assumed to be justified for bed (and free-surface) topographies of small slope. The numerical method described in Stansby & Lloyd (2001) for laminar flow is used. In that paper, a wide range of very complex recirculating and vortex-shedding flows were predicted, at least qualitatively, in oscillatory ambient flows around a conical island of small slope. The method is semi-implicit, second-order accurate in time (mainly) with finite-volume discretization. Numerical diffusion and wave damping are kept to a minimum. This model is extended here to incorporate turbulent flow. Suitable experimental data for validation are available in Lloyd & Stansby (1997, hereinafter referred to as LS), where steady ambient flows around conical islands of small slope were investigated. A desirable feature of these flows is that the wake formation changes dramatically with depth. They are considered to be prominently dependent on a stability parameter $St = C_f D/h$, where C_f is the friction coefficient, D is a representative diameter and h is depth. This follows investigations for vertically sided circular islands by Chen & Jirka (1995, hereinafter referred to as CJ), and also in an atmospheric context by Grubišić, Smith & Schär (1995). Model results presented in LS showed variable agreement with experiment, but the models had various low-order limitations typical of those mentioned above. Note that these experiments have simple boundary conditions. Classical mixing-layer experiments generated by different velocities on either side of a flat plate require careful modelling at the downstream end of the plate with special attention paid to horizontal diffusion from the plate.

The intention of this paper is thus to investigate the influence of horizontal diffusion for a range of recirculating wake flows. The basic hypothesis is that vertical turbulent length scales are different, probably smaller, than the horizontal scales. The emphasis may now be entirely on diffusion as dispersion will be simulated automatically. The mixing-length approach for boundary-layer definition in the vertical is extended to the horizontal by assuming that there is a horizontal mixing length which is a constant multiple of the vertical value at a given elevation, thus giving an eddy viscosity

based on two scales. In this sense, the method may be considered a three-dimensional development of the basic concept of Rastogi & Rodi, now including dispersion and a turbulence model with a simple physical interpretation. There is the usual requirement of turbulence modelling in unsteady flow, that the length scales of the slowly varying flow structures computed directly, recirculations in this case, are much larger than the turbulence length scales. This can only be established *a posteriori* and will be seen to be the case here. Distributions of vorticity and potential vorticity are considered.

2. Mathematical formulation

The continuity and Navier–Stokes equations in Cartesian form are converted to σ coordinates to automatically fit the bed and the moving water surface, enabling high mesh resolution to be produced at the bed for boundary-layer resolution. The σ coordinate is defined as $\sigma = (z - \eta)/h$ where η is surface elevation, h is water depth and z is the vertical coordinate. The velocities in Cartesian coordinates are u, v and w in the x, y and z-directions. In the σ coordinate system $u_\sigma = u, v_\sigma = v, w_\sigma = \omega/h$ (defined below) and the σ subscript is dropped hereinafter for u, v and w. With the assumption for hydrostatic pressure p, $\partial p/\partial\sigma = -\rho g h$, $\partial p/\partial x = \rho g(\partial\eta/\partial x)$ and $\partial p/\partial y = \rho g(\partial\eta/\partial y)$ where ρ is water density and g is acceleration due to gravity.

For local continuity,

$$\frac{\partial\eta}{\partial t} + \frac{\partial(hu)}{\partial x_\sigma} + \frac{\partial(hv)}{\partial y_\sigma} + \frac{\partial\omega}{\partial\sigma} = 0, \tag{1}$$

x momentum,

$$\frac{\partial(hu)}{\partial t} + \frac{\partial(hu^2)}{\partial x_\sigma} + \frac{\partial(huv)}{\partial y_\sigma} + \frac{\partial(\omega u)}{\partial\sigma} = -gh\frac{\partial\eta}{\partial x} + \frac{\partial}{\partial\sigma}\left(\frac{\nu_E}{h}\frac{\partial u}{\partial\sigma}\right) + \frac{\partial}{\partial x}\left(2\nu_E h\frac{\partial u}{\partial x}\right) + \frac{\partial}{\partial y}\left(\nu_E h\left(\frac{\partial u}{\partial y} + \frac{\partial v}{\partial x}\right)\right), \tag{2}$$

and y momentum,

$$\frac{\partial(hv)}{\partial t} + \frac{\partial(huv)}{\partial x_\sigma} + \frac{\partial(hv^2)}{\partial y_\sigma} + \frac{\partial(\omega v)}{\partial\sigma} = -gh\frac{\partial\eta}{\partial y} + \frac{\partial}{\partial\sigma}\left(\frac{\nu_E}{h}\frac{\partial v}{\partial\sigma}\right) + \frac{\partial}{\partial x}\left(\nu_E h\left(\frac{\partial v}{\partial x} + \frac{\partial u}{\partial y}\right)\right) + \frac{\partial}{\partial y}\left(2\nu_E h\frac{\partial v}{\partial y}\right), \tag{3}$$

where kinematic eddy viscosity has turbulent and molecular components such that $\nu_E = \nu_t + \nu$, respectively. Note that advection terms are defined in σ coordinates and horizontal diffusion in Cartesian coordinates; the latter is discussed further below. The vertical velocity is defined by

$$\omega = h\frac{\mathrm{d}\sigma}{\mathrm{d}t} = w - u\left(\sigma\frac{\partial h}{\partial x} + \frac{\partial\eta}{\partial x}\right) - v\left(\sigma\frac{\partial h}{\partial y} + \frac{\partial\eta}{\partial y}\right) - \left(\sigma\frac{\partial h}{\partial t} + \frac{\partial\eta}{\partial t}\right), \tag{4}$$

with $\omega = 0$ when $\sigma = 0, -1$, corresponding to the water surface and the bed.

The depth-integrated continuity equation is given by

$$\frac{\partial\eta}{\partial t} + \int_{-1}^{0} hu\,\mathrm{d}\sigma + \int_{-1}^{0} hv\,\mathrm{d}\sigma = 0. \tag{5}$$

The vertical mesh is compressed close to the bed using semi-parabolic stretching as in Stansby & Lloyd (2001). The mesh size at the bed should be small enough

for $z^+ = (z - z_b)\sqrt{(u_*^2 + v_*^2)}/\nu$ to be less than 5 in the laminar sublayer, so that the no-slip condition may be applied directly at the bed. Here, z_b is the bed elevation and $u_* = \sqrt{\nu(\partial u/\partial z)}$ and $v_* = \sqrt{\nu(\partial v/\partial z)}$ are the friction velocities in the x- and y-directions. Zero stress is imposed at the water surface. The numerical solution method is the same as in Stansby & Lloyd (2001), apart from the treatment of horizontal diffusion, and is summarized below.

It is not possible to use the (local) flux terms hu, hv as general variables since u and v appear in isolation in the vertical and horizontal diffusion and in the vertical advection terms. A staggered mesh is used to avoid checkerboard oscillations within a finite-volume approach. In the momentum equations, second-order Crank–Nicolson ($\theta = 1/2$) time stepping is used for surface elevation gradient terms to obtain the horizontal velocities and fully implicit time-stepping ($\theta = 1$) is used for vertical diffusion. The fully implicit assumption reduces/avoids a time-step limitation owing to the very small vertical cell size at the bed and has been effectively validated in Letherman *et al.* (2000) for a wide range of oscillatory flows. Time stepping for advection and horizontal diffusion is treated explicitly, to second-order accuracy, using the Adams–Bashforth scheme. The upwind QUICK scheme (at least second-order accurate) is used for the spatial discretization of advection, in conservative form, using σ coordinates. Horizontal diffusion is discussed below. Second-order Crank–Nicolson ($\theta = 1/2$) time stepping is used to discretize the depth-integrated continuity equation. The solution method for each time step is thus to substitute the horizontal velocities from the momentum equations into the depth-integrated continuity equation for each horizontal cell. This gives a penta-diagonal equation set for η which is solved by a conjugate gradient method. The flow is thus defined and horizontal velocities may be retrieved.

The velocity derivatives defining the stress terms for 'horizontal diffusion' were previously determined from the Cartesian frame of reference by interpolation from the vertical variations in σ coordinates (Stansby 1997). This avoids certain errors near steep bed slopes. However, this generated errors in this application with a very small vertical bed-cell dimension and horizontal gradients are difficult to resolve in this way. Since we are here concerned with (relatively) small bed gradients, we revert to the formulation for horizontal gradients obtained from the σ coordinate system. For example:

$$\frac{\partial u}{\partial x} = \frac{\partial u}{\partial x_\sigma} - \frac{1}{h}\left(\frac{\partial \eta}{\partial x}(1+\sigma) - \sigma\frac{\partial z_b}{\partial x}\right)\frac{\partial u}{\partial \sigma}, \tag{6}$$

which gives a smooth variation and avoids numerical instability. In the eddy viscosity formula described below, horizontal derivatives are obtained in the same way. The stress gradient terms are finally obtained in a conventional finite-volume formulation (as in Stansby 1997).

3. Turbulence modelling

The mixing-length model has been mainly applied to attached wall boundary layers with a mixing length $l = \kappa(z - z_b)$ for $(z - z_b)/\delta < \lambda/\kappa$ and $l = \lambda\delta$ for $\lambda/\kappa < (z - z_b)/\delta < 1$, where κ is the von Kármán constant, typically 0.41, $(z - z_b)$ is the distance from the wall, δ is the boundary layer thickness and λ is a constant, typically 0.09. In order to return conditions for the viscous sublayer, the mixing length has to be 'damped' close the wall and the standard approach is to use the van Driest formula: $l = \kappa(z - z_b)[1 - \exp(-z^+/A)]$, where $z^+ = u_*(z - z_b)/\nu$ and the

constant $A = 26$. In the case of the shallow-water flows here due to a steady current, the boundary-layer thickness may be assumed to be equal to the water depth h. The eddy viscosity is then defined as $\nu_t = l^2 |\partial u/\partial z|$, e.g. Rodi (1984). In this definition, parallel flow in the x-direction has been assumed for convenience. A finite mixing length at the water surface is, of course, physically unrealistic, but has no effect on vertical diffusion as the zero stress condition is imposed.

There have not been applications of the mixing-length approach to two or three dimensions, to the author's knowledge, but Rodi (1984) suggested a form of the strain rate parameter which is also widely applied in large-eddy simulation (LES). This is given by $S = (2S_{ij}S_{ij})^{1/2}$ and $\nu_t = l^2 S$, where $S_{ij} = \frac{1}{2}(\partial u_i/\partial x_j + \partial u_j/\partial x_i)$ is the rate-of-strain tensor. Note that overbars are often included to represent 'mean' (or filtered in LES terms) quantities, but here we are only concerned with slowly varying ('mean') values and the overbars are omitted. The rate of production of turbulent kinetic energy is given by $P = \nu_t S^2$ and energy transfer is only from the large-scale motions, computed directly, to the small-scale turbulence, which is modelled. We now propose different length scales for horizontal motion l_h and vertical motion, l_v, splitting the rate of strain components for horizontal and vertical turbulence, giving a formula for turbulent viscosity:

$$\nu_t = \left({l_h}^4 \left[2\left(\frac{\partial u}{\partial x}\right)^2 + 2\left(\frac{\partial v}{\partial y}\right)^2 + \left(\frac{\partial v}{\partial x} + \frac{\partial u}{\partial y}\right)^2 \right] + {l_v}^4 \left[\left(\frac{\partial u}{\partial z}\right)^2 + \left(\frac{\partial v}{\partial z}\right)^2 \right] \right)^{1/2}, \quad (7)$$

assuming $(\partial w/\partial z)^2 \ll (\partial u/\partial x)^2 + (\partial v/\partial y)^2$, $\partial w/\partial y \ll \partial v/\partial z$ and $\partial w/\partial x \ll \partial u/\partial z$ for shallow-water flows where vertical velocity w is small. The vertical length scale l_v is the standard form as defined above. The horizontal length scale is different, usually larger, than this and the simplest assumption is to assume direct proportionality defined by $l_h = \beta l_v$. The constant β has to be determined from comparison with experiment. In the case of parallel (or nearly parallel) flow, eddy viscosity reverts to its standard boundary-layer form. With $l_h = l_v$, it reverts to its correct mathematical three-dimensional form (with negligible vertical velocity). Although it has been stated that finite l_v is unphysical at the water surface, finite l_h is not and the basic assumption is that l_h is uniform over most of the water depth.

4. Results

In the experiments of LS, particle tracking velocimetry (PTV) was used to give instantaneous surface velocity vectors with examples of vortex shedding and an almost steady recirculation bubble. The 'conical island' has an 8° slope and a base diameter of 0.75 m. The channel is 1.52 m wide and the bed is horizontal and smooth (painted wood). The depth defining St is adjacent to the island (at a point on a line through the island centre, normal to the flow direction, away from the immediate influence of the island). The 'critical' St value for the onset of a steady recirculating wake is close to 0.4. For the case of a vertically sided island, CJ suggested a critical value of about 0.5 (although reappraisal in Chen & Jirka (1997) suggested a value closer to 0.6). There are differences in the width of the (horizontal) shear layers separating from the islands in the two cases owing to the very different slopes and there are very different ratios of flume-width-to-diameter. For LS it was about $2\frac{1}{2}$ (based on mid-depth diameter) and for CJ it was 10. A further difference between LS and CJ is that, while both refer to unsteady wake bubbles close to the critical value, LS describe low-frequency transverse oscillations of the recirculation zones while CJ show wake instability of

Case	h_{out} (m)	h (m)	D_{mid} (m)	R_h	C_f	Fr	St
1	0.019	0.0200	0.607	1900	0.0085	0.21	0.26
2	0.0145	0.0160	0.636	1450	0.0090	0.23	0.36
3	0.01325	0.0148	0.644	1325	0.0093	0.23	0.405
4	0.012	0.0136	0.652	1200	0.0095	0.26	0.45
5	0.011	0.0129	0.658	1100	0.0097	0.24	0.49
6	0.0065	0.0093	0.676	650	0.0111	0.23	0.80

TABLE 1. For each case, the following parameters are defined: downstream depth, h_{out}; depth adjacent to the island, h; island diameter at mid depth, D_{mid}; depth Reynolds number, $R_h = Uh_{out}/\nu$; friction coefficient, C_f, from the Blasius formula, $C_f = 0.0559\,R_h^{-0.25}$; Froude number, $Fr = U_c/\sqrt{gh}$; and stability parameter, $St = C_f D_{mid}/h$.

relatively high frequency starting at the downstream end of the recirculation zone (for example figure 5*c* in CJ). As the stability parameter is reduced, this becomes rather like vortex shedding referred to in LS.

The flow parameters for the numerical simulations are given in table 1. The outflow depth h_{out} and the inflow flux Uh_{out} are prescribed. $U = 0.1\,\mathrm{m\,s^{-1}}$ for all cases. The depth adjacent to the island h is only known *a posteriori*. The computational domain is 4.52 m long and the island centre is 0.76 m from the upstream end. The bed is horizontal to correspond with experiment where the downstream depth was not recorded. The St values in the simulations thus do not correspond exactly with experiment. St values larger than in the experiments were also modelled (by reducing depth further) to investigate certain effects. The depth Reynolds number, $R_h = Uh_{out}/\nu$, is always much greater than the generally accepted value of 500 required for turbulent flow. The free-stream Froude number, $Fr = U_c/\sqrt{gh}$, where $U_c(= Uh_{out}/h)$ is what the mean velocity at the cylinder centre would be without the cylinder in position, is clearly subcritical. Local values increase, particularly around the cylinder on the upstream side, but remain subcritical; some contour plots are shown below. A horizontal mesh of 300×100 was generally used with 10 cells in the vertical, the cell size at the bed giving $z^+ < 5$. Results (velocity variations with time) with 20 cells were almost identical. Results with a horizontal mesh of 450×150 were very close and examples of superimposed vorticity contours are shown below. At $t = 0$, $u = U$ and $v = 0$ everywhere. Asymmetry was set up by setting the cross-velocity at inflow $v/U = 0.5\sin(\pi t)$ for $t < 1$ s. It will be seen below that $\beta = 6$ shows best agreement with experiment, and surface velocity vector plots are shown in figure 1 for $St = 0.26$, 0.36 and 0.405 with $\beta = 6$, alongside the PTV measurements for $St = 0.27$, 0.35 and 0.40.

Clearly, such snapshots of vortex shedding for the two lower St values can only allow a qualitative comparison, but the size and position of the vortex forming is quite similar in model and experiment. Most significantly, a stable wake has developed close to $St = 0.4$ in both cases and LS reported a downstream stagnation point as far as 1.75 m from the island centre. For the model, this distance is 1.51 m, underpredicting by 14%. In the experiments of CJ, a nearly stable wake formed at $St = 0.5$ and the ratio of this length to diameter was 2.7, the same as that for LS with $St = 0.40$. With $St = 0.39$ (not investigated experimentally), the model produced an unstedy bubble of the kind described in CJ with wake oscillation only at the end of the bubble, an example of which will be shown below.

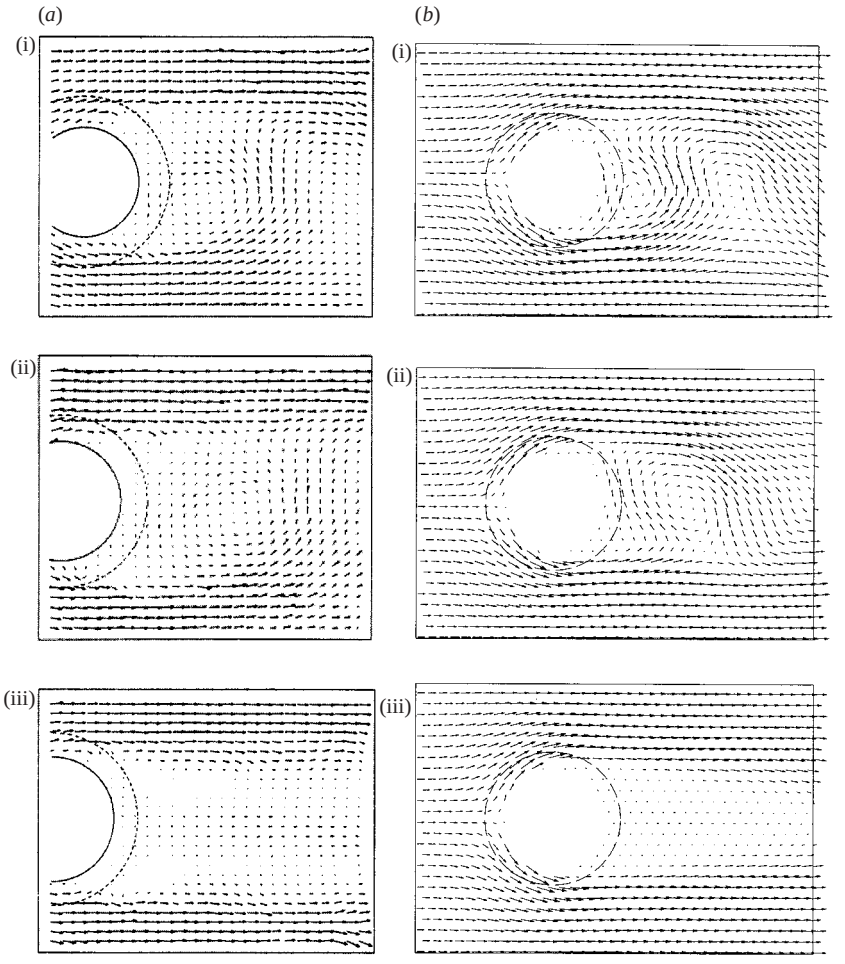

FIGURE 1. (*a*) Surface velocity vectors from the experiments of LS and (*b*) the numerical model with $\beta = 6$. The dashed circle shows the island base (of 0.75 m diameter) in both cases and the full line its intersection with the mean surface level (experiments only). The PTV vector plots were scanned from figure 6 in LS with permission from the American Society of Civil Engineers. (*a*) (i) $St = 0.27$; (ii) 0.35; (iii) 0.40. (*b*) (i) $St = 0.26$; (ii) 0.36; (iii) 0.405.

An assumption of turbulence modelling is that the turbulence length scales are smaller than the larger scale flow structures which are computed directly. The largest horizontal mixing length is about 0.12 m and it can be seen from figure 1 that this is much less than the size of the recirculating zones, justifying the assumption.

The sensitivity of results to β is important. To give a quantitative indicator of unsteady asymmetry, the time variation of cross-flow surface velocity at a distance of 0.73 m downstream of the island centre, on its centreline, was output for all cases. Cross-flow wake fluctuation is generally prominent at this position (if it occurs). Values of this velocity amplitude, after a regular oscillation has become established, are shown in figure 2. It can be seen that the stable wake observed experimentally at $St = 0.4$ is reproduced numerically with $\beta = 6$, with vortex shedding occurring for smaller St values, as observed experimentally.

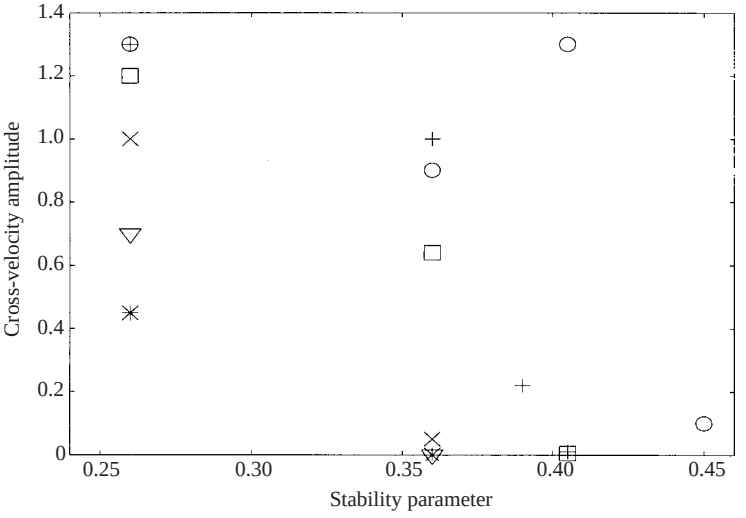

FIGURE 2. Dependence of cross-velocity amplitude, normalized by $U = 0.1\,\mathrm{m\,s^{-1}}$, at $x = 0.73\,\mathrm{m}$ on stability parameter, St, with symbols: ○, $\beta = 4$; +, 6; □, 7; ×, 8; ▽, 9; ✳, 10.

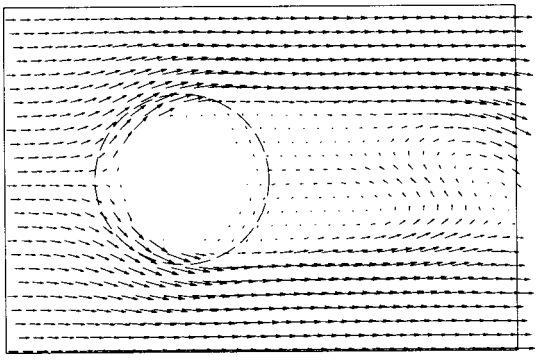

FIGURE 3. Surface velocity vectors from the numerical model with $St = 0.36$ and $\beta = 5$. The dashed circle shows the island base (of 0.75 m diameter).

With $\beta = 4$, a stable wake has formed at $St = 0.49$ with an unsteady bubble at $St = 0.45$ and vigorous vortex shedding for $St = 0.405$ and smaller values. For $\beta = 5$ (not represented in figure 2) a similar unsteady bubble is formed with $St = 0.36$ and 0.405 and a stable wake with $St = 0.45$. A snapshot for $St = 0.36$ is shown figure 3. The vector plot for $St = 0.39$ and $\beta = 6$ was very similar. That an unsteady bubble occurs with $St = 0.36$ and $\beta = 5$ is surprising since vortex shedding occurs with $\beta = 4, 6$ and 7 at this value of St. It was thought possible that the unsteady bubble with $\beta = 5$ may result from the initial conditions. The computation was repeated with no artificial asymmetry and almost identical oscillatory wakes were eventually formed, showing this not to be the case. (This was also found for other cases tested.) In other respects the results are as might be expected. With $St = 0.26$, the velocity amplitude is high and of similar magnitude for $\beta = 4$, 5, 6 and 7 and then decreases as β increases through 8, 9 and 10. For $St = 0.36$, a stable wake has formed with $\beta = 9$ and 10 and an unsteady bubble with $\beta = 8$; lower values have been discussed above. With $St = 0.405$, a stable wake has been shown with $\beta = 6$; there is an unsteady

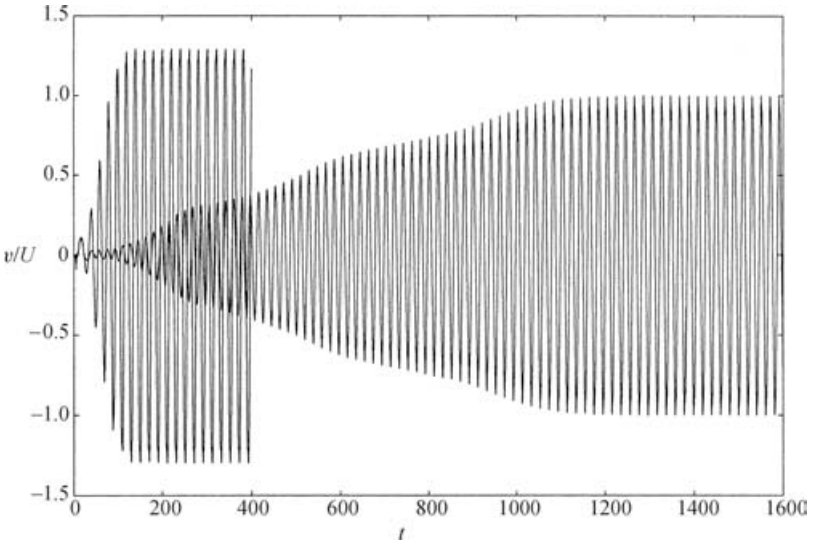

FIGURE 4. Variations of v/U with time t(s) at $x = 0.73$ m, with $\beta = 6$ and $St = 0.26$ (rapidly increasing amplitude) and 0.36 (slowly increasing amplitude).

bubble with $\beta = 5$ and vortex shedding with $\beta = 4$. With $St = 0.45$, there was also an unsteady bubble with $\beta = 4$. For these latter unsteady bubbles, the downstream wake oscillation is less than that shown in figure 3. Increasing the channel width in the model with $St = 0.405$ and $\beta = 6$ to give a width to mid-depth diameter ratio of 4.75 rather than 2.5 still produced a stable wake, indicating that this is not the cause of the different critical St values between LS and CJ. With $\beta = 1$, vigorous vortex shedding occurred for stability parameter values above and below 0.4, with 0.49 the highest value tested. The velocities in the wake showed irregular oscillation in contrast to regular oscillation at higher β values. The special case of $\beta = 0$ is discussed below.

The time to reach a regular wake oscillation is highly dependent on the stability parameter and generally increases as the critical value is approached. This is demonstrated in figure 4 with the cross-velocity time variations for $St = 0.26$ and 0.36 with $\beta = 6$, relating to the results in figure 1. Although the final velocity amplitudes are similar, the times to reach regular oscillation are an order of magnitude different. This is consistent with the experimental observations of LS and CJ.

The linear stability analysis of Chen & Jirka (1997), based on a shallow-water stability (modified Orr–Sommerfeld) equation, gave a critical St value of 0.85, but this necessarily assumes no horizontal diffusion. It is of interest to determine whether a steady recirculating wake is modelled with horizontal diffusion set to zero ($\beta = 0$) if St is high enough. Case 6 in table 1 gives $St = 0.80$ (local to the island) and the fluctuating cross-velocity at $x = 0.73$ m very slowly decays to zero. There are further different basic assumptions between the stability analysis and this model. The effect of channel width, not present in the analysis, has been mentioned. Dispersion is automatically included in the model while velocity is assumed uniform over depth in the analysis. Depth is decreasing downstream in the model (for reasons given above) while it is constant in the analysis. Nevertheless, it is seen that setting horizontal diffusion to zero gives a critical St value about twice that in the experiment and slightly below that determined from linear stability analysis.

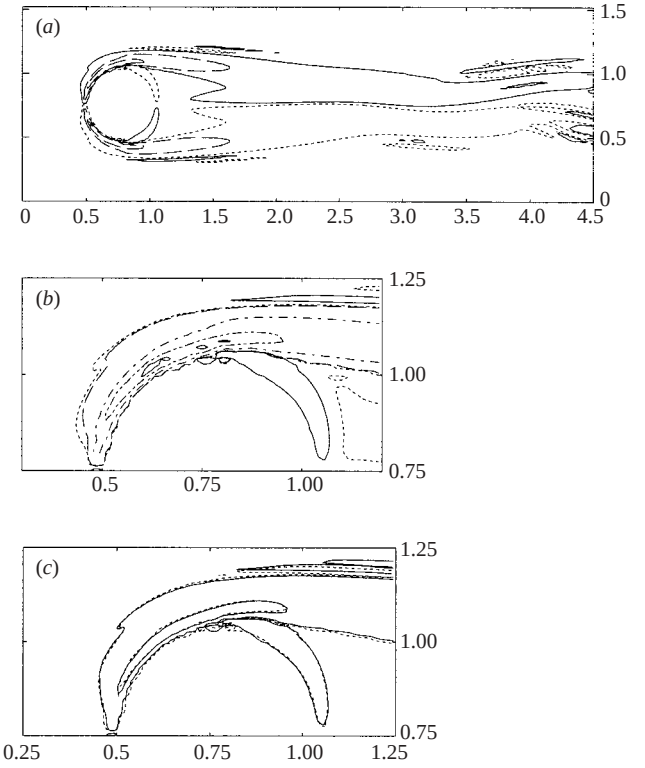

FIGURE 5. Depth-averaged vorticity, $\overline{\omega}$ (s^{-1}), contours for $St = 0.405$ with $\beta = 6$; dimensions are in metres. (*a*) ——, $\overline{\omega} = 0.15; \ldots, -0.1;$ – – –, $\pm 1, \pm 3$. (*b*) ——, $\overline{\omega} = -0.1; \ldots, 0.05;$ – – –, 0.1; — - —, 1; — - - —, 3. (*c*) $\overline{\omega} = -0.1, 0.1, 3;$ ——, 300×100 mesh; – – –, 450×150 mesh.

5. Depth-averaged vorticity, potential vorticity and Froude number

The results above have enabled comparison with experiment. Contour plots of depth-averaged vorticity, Froude number and potential vorticity (defined below) are also significant. Results for the steady case with $St = 0.405$, and the strongly vortex-shedding case with $St = 0.26$, both with $\beta = 6$, are considered.

Figure 5 shows contours of depth-averaged vorticity, $\overline{\omega} = \partial\overline{u}/\partial y - \partial\overline{v}/\partial x$ (with the overbar indicating depth-averaged), for $St = 0.405$; figure 5(*a*) over the whole domain and figure 5(*b*) close to the island. It can be seen that maximum $\overline{\omega}$ magnitudes occur close to the island, but not at the wet/dry intersection. Since $h < 1$ mm is the numerical criterion for dry conditions, the model can only indicate trends as $h \to 0$, but the results do indicate that $|\overline{\omega}| \to 0$ as $h \to 0$. Figure 5(*c*) shows fewer contours with those from the 450×150 mesh overlaid on those for the 300×100 mesh. The results are generally very close. Figure 6 shows contours of depth-averaged vorticity for $St = 0.26$ at $t = 400$ s (a snapshot of vortex shedding) over the whole domain. Vorticity behaviour close to the island on the upstream side is similar to that described above for $St = 0.405$ and vorticities in the shed vortices decrease as they move downstream. Potential vorticity, however, has a more relevant physical interpretation for the latter and contours are shown below.

Figure 7 shows contours of Froude number, $Fr = \sqrt{(\overline{u}^2 + \overline{v}^2)/gh}$, for $St = 0.405$, over most of the wake and close to the island. The maximum value is about 0.6, in the region where $\overline{\omega}$ is also a maximum, which is a marked increase on the free-stream

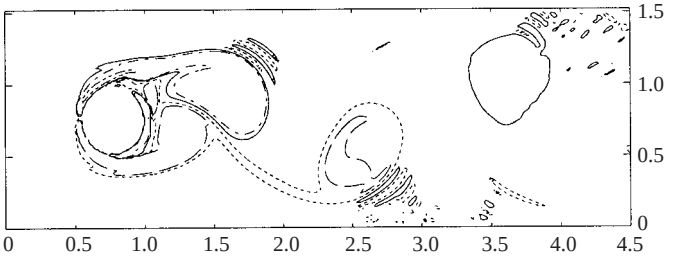

FIGURE 6. Depth-averaged vorticity, $\overline{\omega} = (\mathrm{s}^{-1})$, contours for $St = 0.26$ with $\beta = 6$, at $t = 400\,\mathrm{s}$; dimensions are in metres: – – –, $\overline{\omega} = -0.5; \ldots, -0.2;$ ——, 0.2; — - —, 0.5; - - —, 3.

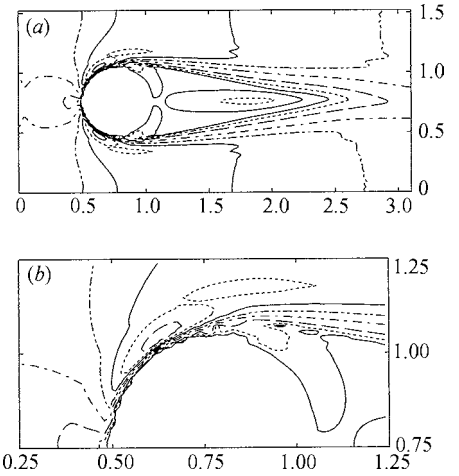

FIGURE 7. Contour plots of Froude number for $St = 0.405$ with $\beta = 6$: at large scale (a) and small scale: ——, $Fr = 0.6$; - - - -, 0.5; ——, 0.4; — - - –, 0.3; – - – -, 0.2; ——, 0.1; - - - -, 0.05; ——, 0.02; (b), with lower values in the wake and near the stagnation point: ——, $Fr = 0.6$; - - - -, 0.5; — - - —, 0.4; — - - —, 0.3; — - —, 0.2; ——, 0.1; - - - - -, 0.05; ——, 0.02. Dimensions are in metres.

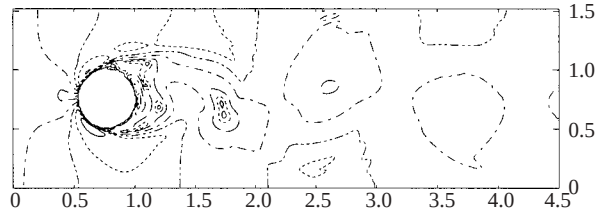

FIGURE 8. Contour plots of Froude number for $St = 0.26$ with $\beta = 6$ at $t = 400\,\mathrm{s}$, with lower values in the wake and near the stagnation point; dimensions are in metres: ——, $Fr = 0.6$; - - - -, 0.4; — - - —, 0.3; — - —, 0.2; ——, 0.1; - - - - -, 0.05; ——, 0.02.

value of 0.23. Figure 8 shows contour plots for $St = 0.26$ over the whole domain; the maximum is now about 0.7, compared with a free-stream value of 0.21. Close to the island, where values are highest, the behaviour is similar to that for $St = 0.405$.

The concept of potential vorticity is widely used in geophysical fluid dynamics in relation to stratified flows and has recently been used to aid understanding of depth-averaged vorticity generation and transport in surf-zone waves, e.g. Peregrine

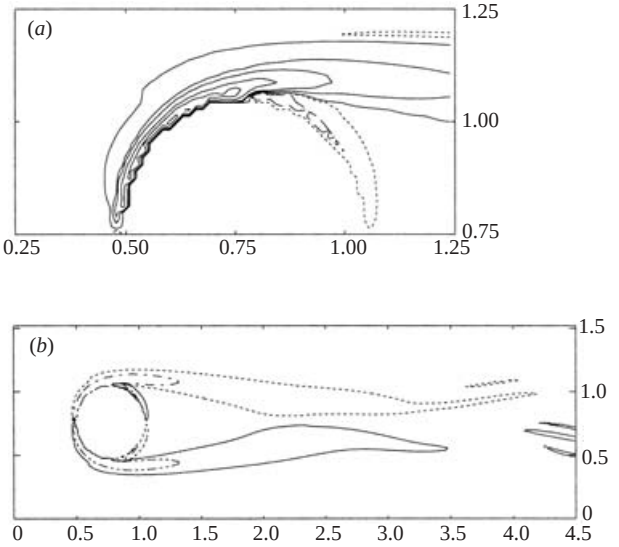

FIGURE 9. Contour plots of potential vorticity at (*a*) small scale and (*b*) large scale, for $St = 0.405$ with $\beta = 6$. Dimensions are in metres. (*a*) – – –, $\overline{\omega}_p = -100; \ldots, -10;$ ——, 10, 100, 200, 500, 1000, 2000 $\mathrm{m^{-1}\,s^{-1}}$ (with values increasing towards wet/dry intersection. (*b*) —·—, $\overline{\omega}_p = -100;$ ——, $-20; \ldots, 20;$ —·—, 100.

(1998). Potential vorticity, $\overline{\omega}_p = \overline{\omega}/h$, is conserved as it is transported in shallow flow, provided it is inviscid. The transport equation for potential vorticity may be derived from the depth-averaged shallow-water equations, which may be written conveniently using vector notation, with the momentum equation in non-conservative form, as

$$\frac{\partial h}{\partial t} + \nabla \cdot (h\overline{\boldsymbol{u}}) = 0, \tag{8}$$

$$\frac{D\overline{\boldsymbol{u}}}{Dt} + g\nabla\eta = \boldsymbol{R}, \tag{9}$$

where bold denotes vector and $\boldsymbol{R}$ represents terms due to bed friction, dispersion and horizontal diffusion. With $\overline{\omega} = \nabla \times \overline{\boldsymbol{u}}$, the equation for potential vorticity may be obtained

$$\frac{D\overline{\omega}_p}{Dt} = \frac{\nabla \times \boldsymbol{R}}{h}. \tag{10}$$

If $\boldsymbol{R} = 0$, $\overline{\omega}_p$ is conserved along a particle path (of depth-averaged form). For increasing h, producing the well-known phenomenon of vortex stretching, $\overline{\omega}$ increases and Kelvin's circulation theorem is satisfied. Of course, $\boldsymbol{R} \neq 0$ in these flows, but the variation of $\overline{\omega}_p$ along a prticle path will give an indication of the importance of viscous/turbulence effects and also of the origin of vorticity. Contours of $\overline{\omega}_p$ are shown close to the island for $St = 0.405$ in figure 9(*a*). The magnitudes are greatest within one cell size of the wet/dry intersection, where $|\overline{\boldsymbol{u}}| \to 0$ and $|\overline{\omega}| \to 0$, as indicated above. In the dry region with $h < 1$ mm, $\overline{\omega_p}$ is set to zero so contour values actually on the intersection are not representative of values as $h \to 0$. However, the highest values are within one cell size of the intersection, indicating that it is an important source of potential vorticity, and hence vorticity, even though the vorticity itself is zero at the

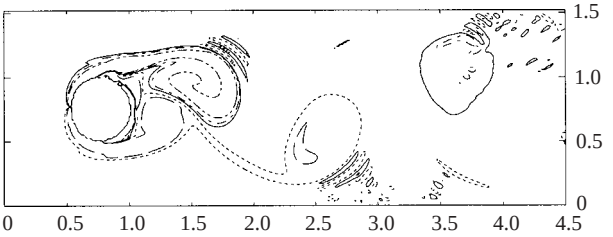

FIGURE 10. Contour plots of potential vorticity, for $St = 0.26$ with $\beta = 6$ at $t = 400$ s. – – –, $\overline{\omega}_p = -30; \ldots, -10;$ ——, 10; — - —, 20; — - - —, 40. Dimensions are in metres.

intersection. Clearly, the nature of such intersections is significant and requires careful modelling. Figure 9(*b*) shows the elongated nature of the wake over whole domain. Figure 10 shows contours for $St = 0.26$ at $t = 400$ s and the magnitude of potential vorticity decays markedly as the shed vortices move downstream, showing the strong influence of dispersion, bed friction and horizontal diffusion. Striations of potential vorticity contours are observed on the downstream outer edges of the shed vortices in figure 10 and in the corresponding vorticity contours of figure 6. For $St = 0.405$, they are also visible on the edge of the wake in figure 5(*a*) and to a lesser extent in figure 9(*b*). Their origin is unclear, but could be associated with weak horizontal shear-layer instability.

6. Discussion and conclusions

A simple two-layer mixing-length model for turbulence has been incorporated in a numerical model for shallow-water flow with negligible numerical diffusion and wave damping. The novel feature is that the horizontal mixing length is explicitly made a multiple of the vertical mixing length within a general three-dimensional eddy-viscosity formulation. This means that the horizontal mixing length and associated strain rates determine the magnitude of eddy viscosity which determines vertical mixing. The present assumption is perhaps the most simple way of making the horizontal turbulence length scale greater than the vertical scale, as has been implicitly assumed previously. It has been demonstrated that this multiple is fundamental to predicting the features of a range of wake structures for flow around an island, exhibiting a transition from vigorous vortex-shedding wakes to steady recirculating wakes as the stability parameter is increased. A multiple of about 6 gives the best agreement. The size of the recirculating wake, when steady with $St = 0.405$, is somewhat underpredicted, the downstream stagnation point being about 14% closer to the island centre than in the experiments. This may be a limitation of the simplistic turbulence modelling approach or it may relate to the assumption of hydrostatic pressure in the shallow-water equations. The latter restricts flow separation in a vertical plane, which becomes more significant as bed slope increases. While the magnitude of depth-averaged vorticity approaches zero at the wet/dry intersection, the magnitude of potential vorticity is at a maximum, indicating the significance of this intersection for generating vorticity even though its magnitude there approaches zero. The Froude number is always subcritical in these flows and at the wet/dry intersection it approaches zero. While this is in contrast to previous assertions that the flow close to the intersection becomes supercritical as depth approaches zero, e.g. Schär & Smith (1993), this appears to assume that the friction coefficient remains

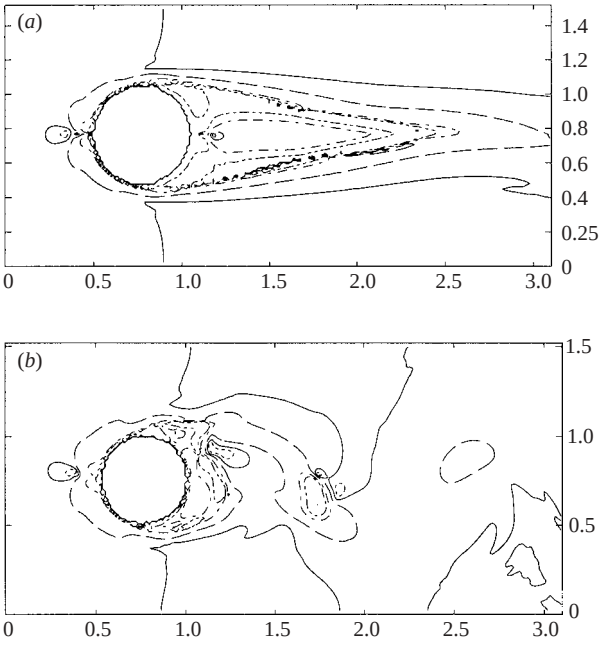

FIGURE 11. Contour plots of friction coefficient, C_f, normalized by the value for onset flow (given by the Blasius formula): (*a*) with $St = 0.405$ and (*b*) with $St = 0.26$ at $t = 400$ s, (both with $\beta = 6$); dimensions are in metres: —- - -—, 10; —- —, 5; – –, 2; ——, 1; - - -, 0.5.

constant. A local friction coefficient is defined by

$$C_f = 2\nu \left(\left(\frac{\partial u}{\partial z} \right)_b^2 + \left(\frac{\partial v}{\partial z} \right)_b^2 \right)^{1/2} \Big/ (\overline{u}^2 + \overline{v}^2),$$

where b denotes velocity gradient at the bed. Contours of this, normalized by the onset flow value (given by the Blasius formula), are shown in figure 11 for the steady case with $St = 0.405$ and the vortex-shedding case with $St = 0.26$ (with $\beta = 6$). Values are clearly much greater than the onset value in the wake regions, including the vortices shed downstream, and increase markedly as the wet/dry intersection is approached; values over 100 times the onset value were computed, but should be treated with caution as both numerator and denominator are very small. C_f is set to zero for depths less than 1 mm so contour values actually on the intersection are not representative of values as $h \to 0$. However, it is clear that vorticity, and associated horizontal mixing, increases C_f above its onset flow value and that it increases to very high values as the intersection is approached where the flow is suppressed from becoming supercritical. Only in a small (stagnation) region just upstream of the island does C_f become less than the onset flow value.

The experiments of LS were made at a relatively small scale. However, this is not expected to be significant since the onset depth Reynolds number, R_h, was greater than 1300 and the accepted lower limit for turbulent flow is about 500. Comparisons with detailed experimental measurements close to the wet/dry intersection would clearly be desirable. Comparisons with experiment are also desirable to determine how the mixing-length ratio might be affected by different geometries or, for example, oscillatory tidal flow. While the flows investigated here have been subcritical, an onset

Froude number of about 0.2 produces a maximum Froude number of about 0.6–0.7 and slightly higher values will probably produce supercritical flow locally, generating surface ripples and/or shocks. Shocks generate vorticity, further complicating the physics and presenting a modelling challenge.

An interesting result from the model concerns the formation of unsteady wake bubbles. The experiments of CJ show relatively high-frequency wake oscillation at the downstream end of a separation bubble for values of St close to the critical and this is also reproduced in the model for certain combinations of St and β. In the experiments of LS, such an unsteady bubble was not observed (although they refer to slowly varying bubble oscillation near the critical St as an unsteady wake bubble) and their results were approximately reproduced in the model with $\beta = 6$. The model did, however, produce such an unsteady bubble with this β at a value of St not investigated experimentally, suggesting that it might have been missed. The model results further suggest that the formation of an unsteady bubble is sensitive to the value of β. In particular, for $St = 0.36$ it occurs with $\beta = 5$ but not with $\beta = 6$ or 4. In complex full-scale flows, there will be additional factors determining this ratio, making precise flow prediction problematic.

This study should further emphasize the limitations of depth-averaged modelling with a constant, or quasi-steady, friction coefficient (or Chézy factor). Horizontal mixing affects the vertical variation of velocity, which in turn affects bed shear. This causes the friction coefficient to be increased where vorticity is present (in wakes in this case). Dispersion is, of course, either omitted, or a standard vertical variation of velocity is assumed which cannot take into account horizontal diffusion. However, this study also shows that, for stability parameters away from the critical, flows with stable wakes or strong vortex shedding are relatively insensitive to horizontal diffusion and suitably calibrated depth-averaged models may have a useful role with the advantage of being very computationally efficient.

The author acknowledges several useful suggestions by the referees, particularly that suggesting potential vorticity. Experimental work on shallow-water flows has stimulated this study and funding from the Engineering and Physical Sciences Research Council is acknowledged. A short version of this paper was included in the International Association for Hydraulics Research Symposium on Shallow Flows, Delft, June, 2003. The PTV vector plots in figure 1 were reproduced with permission from the American Society of Civil Engineers.

REFERENCES

Chen, D. & Jirka, G. H. 1995 Experimental study of plane turbulent wakes in a shallow water layer. *Fluid Dyn. Res.* **16**, 11–41.

Chen, D. & Jirka, G. H. 1997 Absolute and convective instabilities of plane turbulent wakes in a shallow water layer. *J. Fluid Mech.* **338**, 157–172.

Cobbin, A. M., Stansby, P. K. & Duck, P. W. 1995 The hydrodynamic damping force on a cylinder in oscillatory, very high Reynolds number flows. *Appl. Ocean Res.* **17**, 291–300.

Grubišić, V., Smith, R. B. & Schär, C. 1995 The effect of bottom friction on shallow-water flow past an isolated obstacle. *J. Atmos. Sci.* **52**, 1985–2005.

Jirka, G. H. 2001 Large scale structures and mixing processes in shallow flows. *J. Hydraul. Res.* **39**, 567–573.

Letherman, S. B., Cotton, M. A., Stansby, P. K., Chen, C. & Chen, D. 2000 An assessment of $k-\varepsilon$ and $k-l$ turbulence models for a wide range of oscillatory rough bed layers. *J. Hydroinformatics* **2**, 221–234.

Lloyd, P. M. & Stansby, P. K. 1997 Shallow-water flow around model conical islands of small side slope. I: Surface-piercing. *J. Hydraul. Engng ASCE* **123**, 1057–1068.

Peregrine, D. H. 1998 Surf zone currents. *Theoret. Comput. Fluid Dyn.* **10**, 295–309.

Prandtl, L. 1927 Über die ausgebildete turbulenz. *Z. angew. Math. Mech.* **5**, 137–138.

Rastogi, A. K. & Rodi, W. 1978 Predictions of heat and mass transfer in open channels. *J. Hydraul. Engng ASCE* **104**, 397–419.

Rodi, W. 1984 Turbulence models and their applications in hydraulics. *IAHR Monograph*, 2nd edn.

Schär, C. & Smith, R. B. 1993 Shallow flow past isolated topography. Part I. Vorticity production and wake formation. *J. Atmos. Sci.* **50**, 1373–1400.

Stansby, P. K. 1997 Semi-implicit finite-volume shallow-water flow and solute transport solver with $k-\varepsilon$ turbulance model. *Intl J. Numer. Meth. Fluids* **25**, 285–313.

Stansby, P. K. & Lloyd, P. M. 2001 Wake formation around islands in oscillatory laminar shallow-water flows. Part 2. Boundary-layer modelling. *J. Fluid Mech.* **429**, 239–254.